IRSTI 61.67.99 https://doi.org/10.26577/IJBCh20261919

A. El-Hashani[1], K.M. Elsherif[2*], G.F. Musbah[1], A. Imragaa[1], H.F. Emrayed[3]

[1]Department of Chemistry, Faculty of Science, University of Benghazi, Benghazi, Libya
[2]Department of Medical Laboratory Science, Faculty of Health Science, Misurata University, Misurata, Libya
[3]Department of Chemistry, Faculty of Science, Omar Al-Mukhtar University, Al-Bayda, Libya
*e-mail: elsherif27@yahoo.com

CHEMICAL FUNCTIONALIZATION OF PALM FIBERS FOR IMPROVED DYE ADSORPTION: SUSTAINABILITY AND EFFICIENCY

Abstract: The potential of chemically modified palm fibres (CMPF) as effective, economical, and eco-friendly sorbents for wastewater treatment – more specifically, for dye removal – is highlighted in this study. Two adsorbents were produced from palm fibres: acid-base treated palm fibres (A-BTPF), treated with H_2SO_4 and NaOH, and CMPF, treated with CS_2. The addition of xanthate and aldehyde functional groups to CMPF, which enhanced its adsorption ability, was validated by FT-IR analysis. Adsorption behavior was assessed for neutral red (NR) and methyl green (MG) dyes under varying pH, contact time, adsorbent dose, initial dye concentration, and temperature. Both adsorbents demonstrated significant removal efficiencies, with maximum adsorption of NR at pH 4 and MG at pH 10. The enhanced adsorption of MG at basic pH is consistent with the adsorbent's pH_{PZC} value of 9.0. Adsorption data were best described by the Langmuir isotherm model, with maximum adsorption capacities of 19.88 mg/g for NR and 7.45 mg/g for MG, and correlation values of 0.9935 and 0.9869, respectively. Kinetic investigations showed that adsorption followed a pseudo-second-order model (R^2 = 0.9988 for NR and 0.9989 for MG). Thermodynamic analysis confirmed that the process was spontaneous and endothermic (negative $\Delta G°$ and positive $\Delta H°$ values). CMPF exhibited superior adsorption efficiency and capacity compared to A-BTPF, demonstrating its suitability as a high-performance, sustainable biosorbent for wastewater treatment. Given its low cost, abundance, and enhanced adsorption performance, CMPF has strong potential for industrial-scale applications, particularly in textile, pharmaceutical, and dye-producing industries, offering a green alternative to conventional adsorbents in water purification.

Keywords: Biosorption, Xanthated palm fiber, Dye removal, Wastewater treatment, Adsorption isotherms, Adsorption kinetics.

Introduction

The textile, food, cosmetics, and paper industries release large amounts of dyes into the environment annually, which can prove harmful to ecosystems and human health. An estimated 10–15% of the more than 1,000 tonnes of commercially available colours used in the textile industry alone end up in wastewater systems, largely untreated (Al-Saeedi et al., 2023; Elsherif, Yaghi, 2017; Ibrahim et al., 2021). About 60–70% of the world's dye output, which surpasses 700,000 tonnes per year, is composed of azo dyes, which are highly preferred because of their ease of synthesis and stability (Djama et al., 2023; Pietrzyk et al., 2023). Synthetic dyes have complex, durable structures that resist biodegradation, persisting in aquatic environments. Their stability threatens ecosystems and human health by depleting oxygen, harming aquatic life, and causing mutagenic and carcinogenic effects (Alkherraz et al., 2023; Alshorifi et al., 2022; Elsherif et al., 2019). Commonly used dyes like Rhodamine B, methyl green, methylene blue (MB), neutral red, Congo red, and Reactive Black-5 can be anionic, neutral, or cationic (Alardhi et al., 2023; El-Shafie et al., 2023). Their persistent discharge – particularly from textile wastewater – threatens human health and the environment, challenging conventional water treatment methods (El-Hashani et al., 2018b). These toxic, non-biodegradable dyes disrupt microbial ecosystems and, with prolonged exposure, may cause cancer or skin irritation in humans (El-Hashani et al., 2018a; Fito et al., 2023).

The growing global emphasis on advanced wastewater treatment underscores the urgent need for effective industrial dye waste management (Hammad et al., 2024; Harouache et al., 2024; Tenev et al., 2023). Despite various existing methods – such as membrane separation (Elsherif et al., 2014a; Huang et al., 2024), adsorption (Alkherraz et al., 2020b; Islam et al., 2024; Matić et al., 2024; Olusegun et al., 2023), photocatalytic oxidation (Zhou et al., 2024), electrochemical techniques (Bibikov et al., 2024; Elsherif et al., 2014b), biopolymer sorption (Lakshmi et al., 2024), and biodegradation (Nasiri et al., 2023) – water pollution remains a critical environmental challenge (Rashid et al., 2021). Among these, adsorption stands out for its efficiency, cost-effectiveness, ease of implementation, and versatility in removing diverse pollutants (Alkherraz et al., 2020a).

Activated carbon is widely used for adsorption due to its high surface area and capacity, but its high cost limits large-scale applications (Devi et al., 2023; Sghiouri Idrissi et al., 2024). Researchers are exploring low-cost alternatives like biosorbents derived from natural materials, including coffee grounds, cellulose, and algae (Elsherif et al., 2022). Carbonized coffee grounds show promise for removing pollutants like bisphenol A due to their porous structure (Elsherif et al., 2018a; Memetova et al., 2023), while cellulose and algal biomass effectively adsorb heavy metals (e.g., Pb, Cd, Zn) (Li et al., 2021). Microalgae, with their large surface area, can capture diverse contaminants (Wang et al., 2021). Agricultural wastes (e.g., rice husks, sugarcane bagasse, pine leaves) achieve >90% removal efficiency for dyes (methylene blue, reactive orange, rhodamine B) at 5–300 mg/L concentrations, proving viable as activated carbon substitutes (Elsherif et al., 2018b; Gutiérrez et al., 2021; Hamedi et al., 2023; Sanou et al., 2024).

Researchers continue exploring sustainable, low-cost adsorbents with favorable surface properties and regeneration potential for large-scale water treatment. Palm trees, abundant in tropical regions like the Middle East, offer promising solutions. Libya alone hosts ~20 million palms across 23,000 hectares, yielding over 20 kg of dry residues per tree annually (Racchi & Camussi, 2018). Palm fiber's high functional group density (especially from southern Libya) enhances its adsorption capacity, making it an eco-friendly biosorbent (Geddeda & Abdassalam, 2010). Modified date palm residues have demonstrated effective removal of heavy metals and dyes (Din et al., 2024; Melliti et al., 2021; Rambabu et al., 2021), positioning them as sustainable alternatives for industrial wastewater treatment.

This study evaluates sustainable, bio-based sorbents from palm fibres for dye removal in water treatment. We compare the adsorption performance of Acid-Base Treated Palm Fibres (A-BTPF) and Chemically Modified Palm Fibres (CMPF), prepared via H_2SO_4/NaOH and CS_2 treatments respectively. FTIR confirmed C-S group formation in CMPF, enhancing adsorption capacity. Batch experiments analyzed removal efficiency under varying conditions (pH, temperature, dose, contact time, concentration). Adsorption mechanisms were characterized through kinetic, isotherm, and thermodynamic studies. Results demonstrate CMPF's superior performance as an eco-friendly alternative to conventional sorbents.

Materials and methods

Neutral Red (NR), Methyl Green (MG), sodium hydroxide, hydrochloric acid, sulphuric acid, and carbon disulphide were among the analytical-grade chemical reagents that were purchased from Merck Darmstadt, Germany. They were used without any additional purification. Figure 1 shows both the NR and MG dyes' chemical structures. Double-distilled water was utilized to prepare all solutions.

Figure 1
Structure of dyes: (a) methyl green (b) neutral red (Al-Saeedi et al., 2023; Ibrahim et al., 2021)

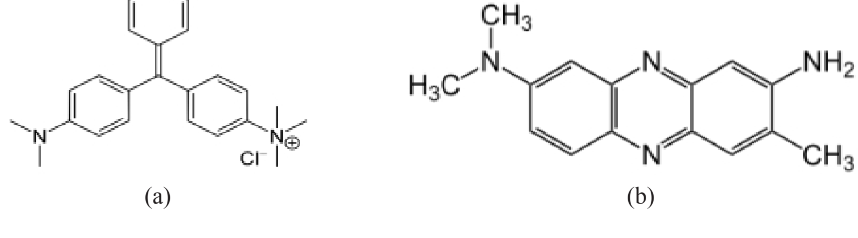

(a) (b)

Preparation of adsorbent materials: Palm fibers were sourced from Galu City, southern Libya. The fibers were initially cut into 1 cm segments, followed by thorough washing with double-distilled water (DDW) to eliminate impurities. Subsequent drying at 150 ± 2°C for 48 hours and cooling to room temperature were performed.

To prepare the first adsorbent material, the dried fibers were ground and sieved to obtain particles smaller than 75 μm and this material is designed as dry palm fiber powder (DPFP). A 50 g sample of this powder was subjected to acid treatment using 100 ml of 4 M H_2SO_4 for 60 minutes, followed by overnight incubation. This acid treatment facilitates ring-opening reactions, as reported by Homagai et al. (2010). After being acid-treated, the material was cleaned with DDW to remove any remaining excess acid, and then dried at 70 ± 2°C. Lastly, 200 ml of 4 M NaOH solution was added to 25 g of the acid-treated powder, agitated for 60 minutes, and then left overnight. The resulting product, labelled as Acid-Base Treated Palm Fibers (A-BTPF), was filtered, washed, and dried at 70 ± 2°C.

To prepare the second adsorbent material, the previously obtained A-BTPF was further treated with 25 ml of CS_2, stirred for 3 hours, and allowed to stand overnight. The resulting product was filtered, washed, and dried at 70 ± 2°C. This chemically modified material, labelled as Chemically Modified Palm Fibers (CMPF), was employed as an adsorbent. The synthetic procedure for CMPF was adapted from Pathania et al., 2017.

Characterization of adsorbent materials: FT-IR spectroscopy of the DPFP, A-BTPF, and CMPF adsorbents was carried out using an FT-IR Spectrometer fitted with a universal ATR sample attachment from PerkinElmer.

The Point of Zero Charge (pH_{PZC}) is the pH at which the net surface charge of the adsorbent becomes neutral, meaning the positive and negative surface charges are balanced. This property indicates the acidic or basic nature of the adsorbent surface. Below the pH_pzc, the surface carries a positive charge, while above it, the surface is negatively charged.

The Madadgar et al. (2023) method was used to determine the pH_{pzc}. In six Erlenmeyer flasks, 50 mL of a 0.01 M NaCl solution and 0.15 g of the biosorbent was mixed. The proper amounts of HCl or NaOH were added to each mixture to adjust its pH down to 2, 4, 6, 8, 10, and 12. Each mixture was shaken for 24 hours at room temperature before its final pH was determined. The pH_{pzc} was identified as the point of intersection of a plot that showed the change in final pH vs beginning pH.

Dyes adsorption efficiency and capacity: The adsorption behavior of methylene green and neutral red onto both A-BTPF and CMPF adsorbent materials was examined and assessed by determining the adsorption efficiency (%E) and adsorption capacity (Q_e) using the following equations (Elsherif et. al., 2017):

$$Q_e = \frac{(C_0 - C_e) * V}{M} \quad (1)$$

$$\%E = \frac{(C_0 - C_e)}{C_0} * 100 \quad (2)$$

where V is the solution's volume in L; M is the mass of the adsorbent material in g; Q_e is the amount of adsorbed dye in mg/g; C_o is the initial dye concentration in mg/L; and C_e is the equilibrium dye concentration in mg/L. UV-Vis spectrophotometry (Molecular Absorption Spectrophotometer 6305 from JENWAY) was used to measure the dyes concentrations both before and after adsorption. In an aqueous solution with defined initial and equilibrium concentrations, a decline in adsorption was observed at 540 nm for NR and at 640 nm for MG. A calibration curve was used to convert the adsorption to concentration.

Adsorption experiments: Batch adsorption studies evaluated NR and MG dye removal using A-BTPF and CMPF, examining key parameters (contact time, adsorbent dose, pH, initial concentration, temperature) as outlined in Table 1. Each trial combined a fixed adsorbent mass with 50 mL dye solution in 100 mL Erlenmeyer flasks, agitated at 150 rpm in a water bath shaker. pH adjustments used HCl/NaOH solutions. After reaching equilibrium, samples were filtered and analyzed via UV-Vis spectrophotometry at λ_{max} to determine residual dye concentrations, enabling calculation of removal efficiency and adsorption capacity.

Table 1
Operating Condition Variations for Adsorption Experiments

Investigated parameter	Variation range
Reaction time (min)	15 – 90
pH	2.0 – 7.0* 2.0 – 12.0**
Adsorbent mass (g)	0.02 – 0.14
Initial dye concentration (ppm)	9.0 – 18.0* 4.5 – 8.5**
Temperature (K)	298 – 318

**for NR dye, **for MG dye*

Equilibrium isotherms and kinetic investigations: The adsorption of NR and MG onto CMPF was analyzed using linear isotherm and kinetic models (Table 2) for initial concentrations (9-18 mg/L) and contact times (15-90 min). These models, with their equations and parameters, helped identify the adsorption mechanism and determine the best-fitting model for our system.

Table 2

Equations and Parameters of Isotherm and Kinetic Models (Alkherraz et al., 2023; Dural et al., 2011; Elsherif et al., 2019; Elsherif et al., 2020; Hammad et al., 2024)

Isotherms Models			
Model	Linear equation	No.	Parameters
Langmuir	$\frac{1}{Q_e} = \frac{1}{Q_m} + \frac{1}{bQ_mC_e}$	(3)	Q_e (mg/g): adsorption capacity C_e (mg/L): Equilibrium concentration b (L/mg): Langmuir constant Q_m (mg/g): Maximal adsorption capacity
Freundlich	$\log Q_e = \log K_F + \frac{1}{n}\log C_e$	(4)	K_F (mg/g (L/mg)1/n): Freundlich adsorption constants n: Empirical constant
Temkin	$Q_e = B_T \ln K_T + B_T \ln C_e$	(5)	B_T (J/mol): Temkin adsorption constant K_T (L/mg): Temkin isotherm constant
D-R	$\log Q_e = \log Q_m - \beta\,\varepsilon^2$ $\varepsilon = RT\log\left(1 + \frac{1}{C_e}\right)$	(6) (7)	B (mol^2/J^2): D-R constant ε (J/mol): Polanyi potential R (kJ/mol K): Gas constant T (K): absolute Temperature
Kinetic Models			
Model	Linear equation	No.	Parameters
Pseudo-first-order	$\ln(Q_e - Q_t) = \ln(Q_e) - \frac{k_1}{2.303} * t$	(8)	Q_t (mg/g): Capacity at t time k_1 (min^{-1}): Adsorption rate constant
Pseudo-second-order	$\frac{t}{Q_t} = \frac{1}{k_2 * Q_e^2} + \frac{1}{Q_e}$	(9)	k_2 (g/mg.min): Adsorption rate constant.
Intra-particle diffusion	$Q_t = k_d t^{1/2} + C$	(10)	k_d (mg/g $min^{1/2}$): Intraparticle diffusion rate constant
Elovich equation	$Q_t = \frac{1}{\beta}\ln(\alpha\beta) + \frac{1}{\beta}\ln t$	(11)	β (g/mg): Amount of surface covering and activation energy α (mg/g min): Initial sorption rate

Thermodynamic investigation: The analysis of thermodynamics is crucial to understanding adsorption processes because it provides significant insights into the spontaneity, sustainability, and nature of the adsorption interactions. Key thermodynamic parameters that impact the total energy dynamics that can be calculated to assess the favorability of the adsorption process include Gibbs free energy (ΔGº, kJ/mol), entropy change (ΔSº, J/mol.k), and enthalpy change (ΔHº, kJ/mol). These parameters can be determined via the following formulas (Alkherraz et al., 2023), which allow for a comprehensive evaluation of the process's thermal characteristics:

$$\Delta G = \Delta H - T\,\Delta S \quad (12)$$

$$\Delta G = -RT \,Ln\, K_d \quad (13)$$

To accurately determine the apparent equilibrium constant of adsorption (K_d), it is essential to use the standard thermodynamic equilibrium constant calculated based on activity, rather than concentration, to reflect the true thermodynamic behavior of the system (Alkherraz et al., 2020b):

$$K_d = \frac{Q_e}{C_e} \quad (14)$$

The interrelationship between entropy, enthalpy, and the distribution coefficient (K_d) is presented by Van't Hoff equation (Alkherraz et al., 2020b), illustrating how these factors collectively contribute to the adsorption mechanism:

$$\ln K_d = \frac{\Delta S}{R} - \frac{\Delta H}{RT} \quad (15)$$

Results and discussion

Adsorbent characterization

FTIR spectra: FTIR spectroscopy was used for analysing chemically modified palm fibres (CMPF), acid-base treated palm fibres (A-BTPF), and dried palm fibre powder (DPFP). A prominent absorption band was seen in all samples (Figures 2a, 2b, and 2c) at about 1020 cm⁻¹. This band was likely caused by inorganic silicates found in the palm fibre samples and might be ascribed to either C–O stretching vibrations or Si–O vibrations. Furthermore, in each case, a broad peak at 3351 cm^{-1} that corresponded to O–H stretching vibrations was seen. The hydroxyl (OH) groups on the carbon surface and any remaining moisture may be partially responsible for this peak.

Figures 2a, 2b, and 2c show the FT-IR spectra of palm fibre adsorbents that were processed differently, such as DPFP, A-BTPF, and CMPF. The structural and chemical alterations brought about by the different treatments are highlighted in the analysis.

Figure 2
Characterization of different adsorbents by FTIR

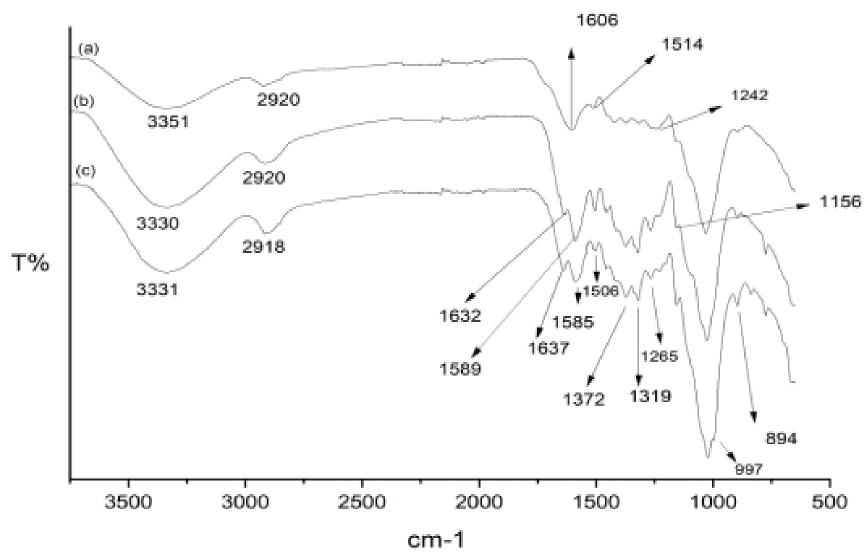

Aromatic, C–C, C–O, and C–O–C groups are present in the DPFP spectrum (Figure 2a), which is typical of characteristics derived from plants. The C–C stretching vibrations are represented by a band at 1606 cm^{-1}, the C–O stretching vibrations by a band at 1514 cm^{-1}, and the C–O–C and aromatic stretching vibrations by a band at 1242 cm^{-1}. These are significant absorption peaks. These peaks confirm the inherent structural properties of the untreated palm fibre.

The A-BTPF spectrum (Figure 2b) reveals significant structural modifications, with original DPFP peaks shifting to higher wavenumbers (1589, 1504, and 1265 cm^{-1}) and new aldehyde group vibrations appearing at 1632 (C=O), 1372, and 1319 cm^{-1} (C-O). These changes confirm the acid-base treatment successfully introduced new functional groups, altering the palm fiber's chemical properties.

The CMPF spectra (Figure 2c) reveal successful xanthation, evidenced by new C–S (997 cm^{-1}) and C=S (894 cm^{-1}) stretching vibrations. The C=S group further confirms xanthate incorporation through a broad absorption band (1632–1156 cm^{-1}), demonstrating effective chemical modification of the palm fiber.

pH at the point of zero charge: The pH_{PZC} (point of zero charge), where the adsorbent surface maintains charge neutrality, was ~9.0 for DPFP (Figure 3). Below this pH, the surface becomes positively charged; above it, negatively charged (Abate et al., 2023; Caldeira et al., 2018).

Figure 3
Point of zero charge (pH_{pzc}) for DPFP

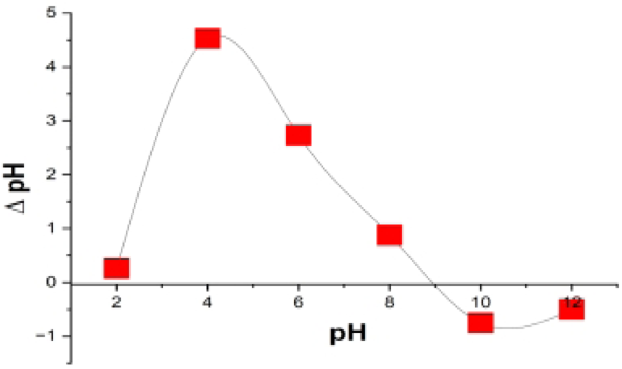

The pH_{PZC} critically influences adsorption behavior. Above pH 9.0, DPFP's negatively charged surface enhances cationic dye uptake. This explains methyl green's (MG) increased adsorption at higher pH, as its protonated amine groups (Figure 1) facilitate electrostatic attraction to the adsorbent surface.

On the other hand, the adsorption behaviour varies for neutral dyes like neutral red. Neutral red is protonated in acidic solutions, which causes the dye molecules and hydronium ions to compete for the adsorption sites on the adsorbent. The adsorption effectiveness may be decreased by this competition, emphasising the need of pH optimisation for various adsorbate types (Ben-Ali et al., 2017).

Effect of pH: Solution pH critically influences dye adsorption by modifying surface charges and adsorbent-dye interactions (Alver et al., 2020; Madadgar et al., 2023). For neutral red (NR), both removal efficiency (%R) and adsorption capacity (Q_e) increased with pH, peaking at pH 4. As shown in Figures 4A & 4B, CMPF achieved 72% removal while A-BTPF reached 61% at this optimal pH.

Removal efficiency and dye uptake declined as pH increased beyond 4 (Figure 4B), consistent with previous reports (Xu et al., 2006). At pH < 4, excessive surface protonation hindered dye ion access. CMPF capacity decreased from 10 to 7.8 mg/g (pH 3-7), while A-BTPF dropped from 7.7 to 6.6 mg/g. This reduction stems from deprotonation in alkaline conditions, creating electrostatic repulsion between dye molecules and the adsorbent surface (Ramesha, 2011). Additional adsorption mechanisms included hydrophobic interactions, van der Waals forces, and hydrogen bonding.

Figure 4 (C and D) illustrates how the methyl green (MG) dye's removal percentage (%R) and adsorption capacity (Q_e) increased with pH, peaking at pH 10 for both A-BTPF and CMPF. At this pH, CMPF and A-BTPF had the highest removal efficiencies of 68% and 61%, respectively, indicating that a basic medium is the best option for adsorption. Since there were no discernible variations in the biosorption capability above pH 10, further research was conducted at this pH.

The pH_{PZC} (9.0) governs MG dye adsorption by controlling surface charge. Below pH 9.0, protonation creates a positively charged surface that repels cationic MG, reducing uptake. Above pH 9.0, deprotonation generates negative surface charges that enhance electrostatic attraction to MG, significantly improving adsorption efficiency, as demonstrated by Belgacem et al. (2022).

Further evidence that CMPF continuously demonstrated greater removal efficiency and biosorption capacity than A-BTPF across all pH levels can be found in Figures 4A, 4B, 4C, and 4D. This demonstrates how the biosorption capabilities of palm fibre for neutral red dye were successfully improved by CS_2 treatment.

Effect of adsorbent dose: Adsorbent dosage significantly influences dye removal efficiency by determining available adsorption sites for a given dye concentration (Elsherif et al., 2024a). Figure 5 (A-D) demonstrates the relationship between biosorbent dose and dye uptake capacity.

The study revealed an inverse relationship between adsorbent dosage and removal efficiency. At the lowest tested dose (0.02 g), A-BTPF and CMPF achieved 70% and 81% NR removal, and 84% and 91% MG removal, respectively. This enhanced performance at lower doses (≤0.14 g) results from greater surface area availability and unoccupied active sites, consistent with Abuzerr et al. (2018).

Conversely, as the adsorbent dose increases, the adsorption capacity decreases. The decline is most likely due to particle aggregation, which reduces the surface area available for adsorption and reduces the efficacy of dye removal (Elsherif et al., 2024b).

Figure 4

Effect of pH on adsorption of NR (A & B) and MG (C & D) onto both A-BTPF and CMPF biosorbents

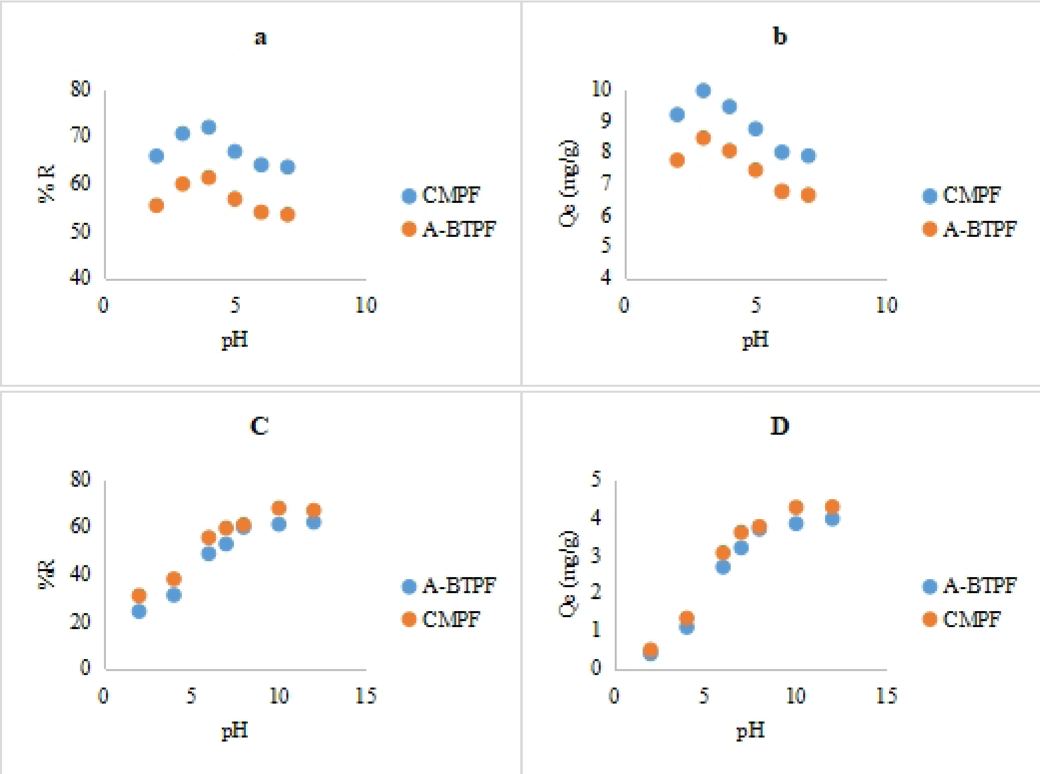

Effect of contact time: Contact time significantly affects adsorption equilibrium between dyes and biosorbents. Tests with A-BTPF and CMPF at 15–90-minute intervals (Figure 6A-B) revealed peak removal efficiencies at equilibrium: 75% (MG) and 65% (NR) for A-BTPF versus 83% and 76% for CMPF. Prolonged contact beyond this point marginally reduced removal rates, suggesting optimal adsorption times.

The results align with Ansari and Mosayebzadeh's findings (2010), demonstrating increasing dye removal with contact time until equilibrium, beyond which additional time yields diminishing returns. Adsorption occurs rapidly initially, then slows as active sites become occupied.

CMPF showed rapid adsorption within the first hour, followed by equilibrium plateauing as active sites became saturated (Alkherraz et al., 2022). Extended contact led to negligible additional uptake, suggesting potential desorption. Optimal contact times were established at 45 minutes for NR and 60 minutes for MG in subsequent tests.

Effect of initial concentration: Initial dye concentration significantly affects removal efficiency by influencing interactions with adsorbent active sites. Studies examined MG (4.5-8.5 ppm) and NR (9-18 ppm) adsorption on A-BTPF and CMPF, with results shown in Figures 7A-D.

Both removal efficiency (%R) and adsorption capacity (Q_e) of NR dye increased with concentration up to 13.5 ppm. For MG dye, CMPF achieved 75% removal (5.5 mg/g) versus A-BTPF's 65% (4 mg/g). These results agree with Alardhi et al. (2023), demonstrating enhanced adsorption at higher concentrations due to increased driving force. The enhanced adsorption at higher concentrations stems from stronger electrostatic dye-adsorbent interactions. However, MG adsorption plateaued above 6.5 ppm due to site saturation, consistent with Pietrzyk et al. (2023), who attributed superior low-concentration removal to higher site availability. Across all tests, CMPF outperformed A-BTPF in both removal efficiency and capacity, confirming its superior biosorbent performance for NR and MG dyes.

Figure 5
Effect of adsorbent dose on adsorption of NR (A & B) and MG (C & D) onto both A-BTPF and CMPF biosorbents

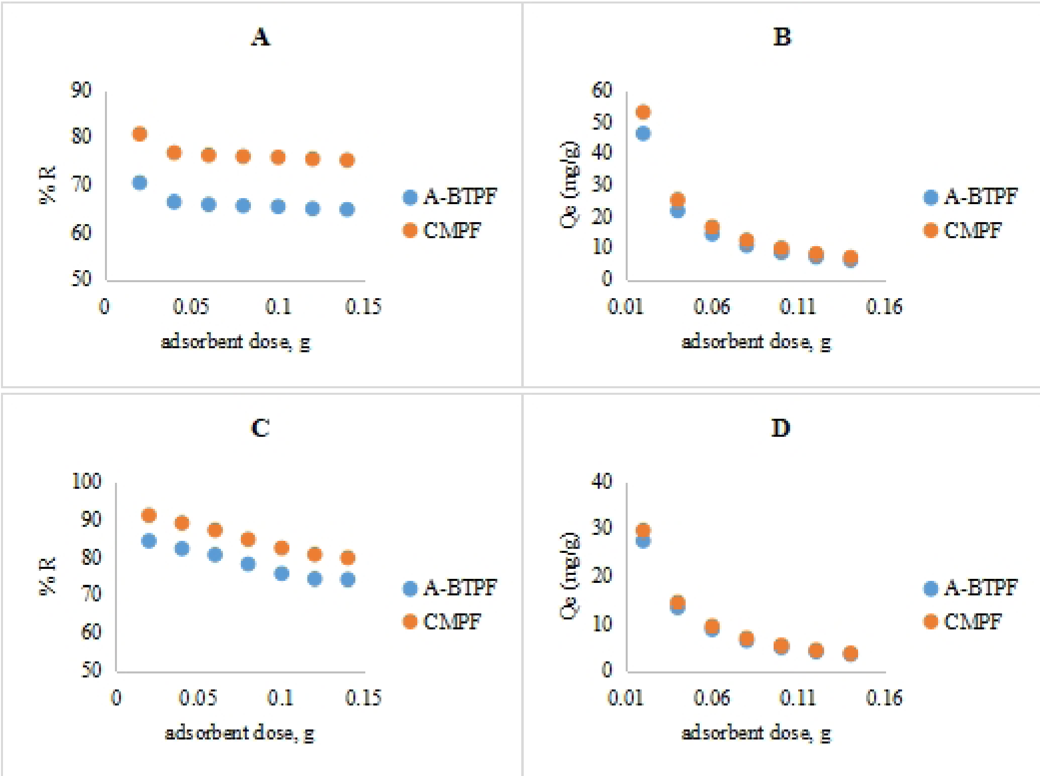

Figure 6
Effect of contact time on adsorption of NR (A) and MG (B) onto both A-BTPF and CMPF biosorbents

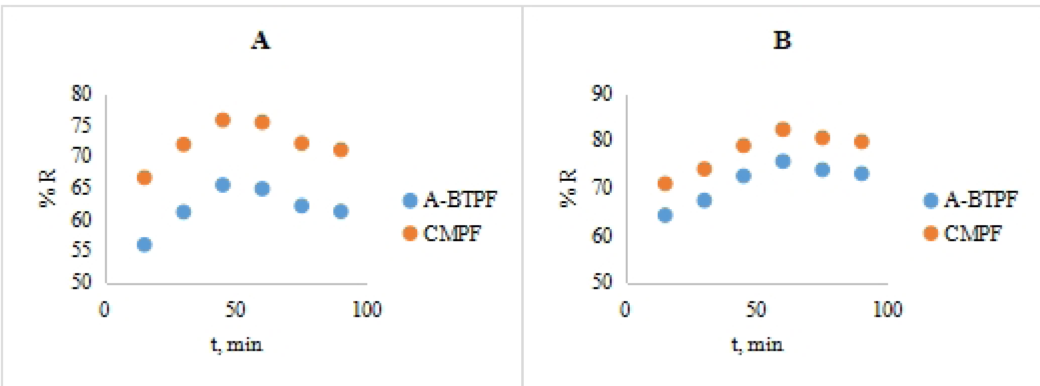

Figure 7
Effect of initial dye concentration on adsorption of NR (A & B) and MG (C & D) onto both A-BTPF and CMPF biosorbents

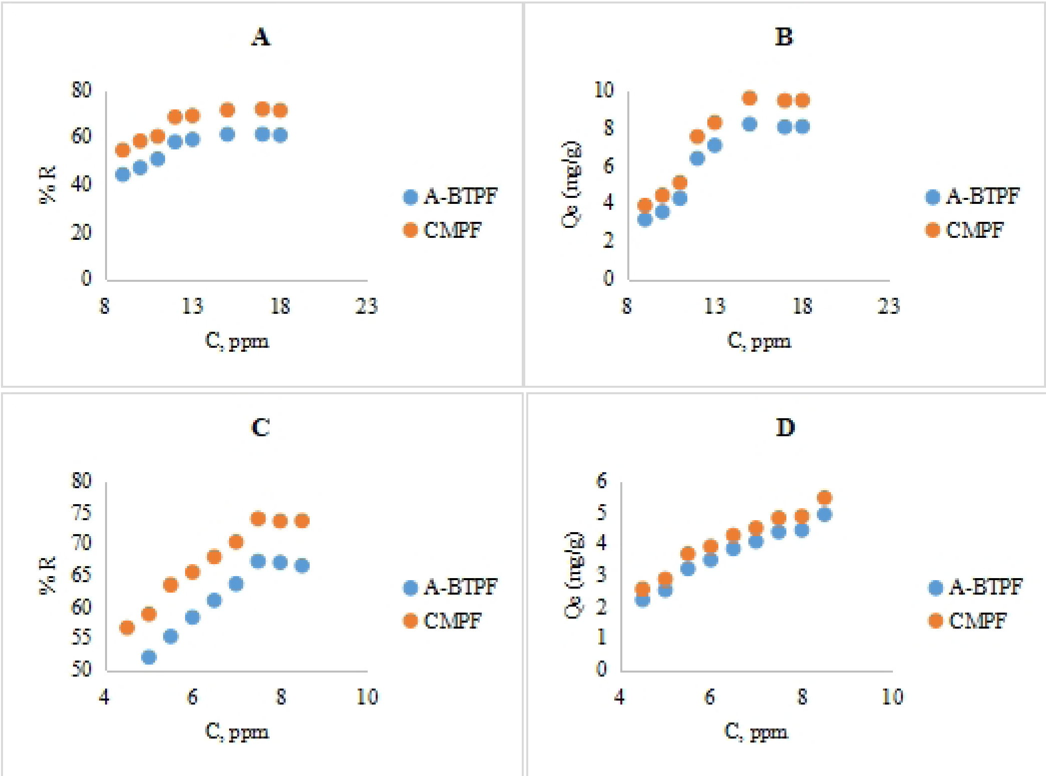

Effect of temperature: The influence of temperature on adsorption capacity is governed by both adsorbent characteristics and experimental conditions, reflecting either endothermic or exothermic behavior (Budi et al., 2018; Elsherif et al., 2024b). Our batch experiments (25-45°C) demonstrated a gradual improvement in removal efficiency with increasing temperature (Figures 8A-B). For neutral red (NR), A-BTPF showed an increase from 70% to 74% removal, while CMPF improved from 81% to 84%. Similarly, methyl green (MG) removal rose from 84% to 86% for A-BTPF and from 90% to 93% for CMPF over the same temperature range, confirming the endothermic nature of the process (Abate et al., 2023). This modest temperature dependence suggests physical adsorption dominates, where enhanced molecular mobility facilitates access to active sites. However, the relatively small effect indicates that other factors – particularly dye chemistry and adsorbent surface properties – play more significant roles in determining adsorption efficiency (Alkherraz et al., 2023; Hammad et al., 2024; Olusegun et al., 2023).

From the previous investigations, carbon disulphide (CS_2)-treated palm fibre showed a notable increase in adsorption capacity for Neutral Red dye following the optimisation process. CMPF's exceptional performance highlights its potential as a strong biosorbent. Accordingly, we will concentrate on examining equilibrium isotherms in order to better understand its adsorption behaviour. These are important indicators of the adsorbent's surface characteristics, adsorption capacity, and interaction mechanisms.

Figure 8
Effect of temperature on adsorption of NR (A) and MG (B) onto both A-BTPF and CMPF biosorbents

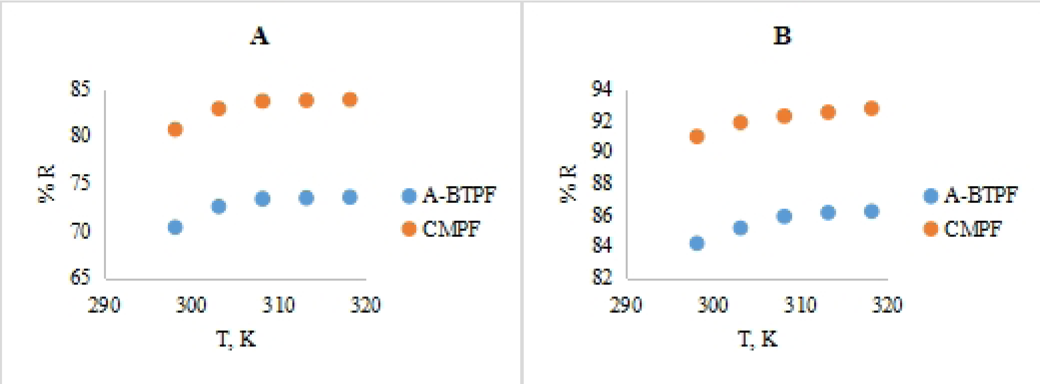

Equilibrium adsorption isotherms: Understanding the adsorption mechanism and designing and optimising adsorption systems depend heavily on equilibrium data, which are typically represented by adsorption isotherms. The most popular isotherm models were used in this investigation to assess the chemically treated palm fiber's (CMPF) adsorption capabilities. Among the models utilised are: The Freundlich isotherm, which provides information about the maximum adsorption capacity, the Langmuir isotherm, which assumes monolayer adsorption onto a surface with a finite number of identical sites; the Temkin isotherm, which describes adsorption on heterogeneous surfaces and indicates the adsorption intensity and capacity; the Dubinin-Radushkevich (D-R) isotherm, which takes into account the effects of indirect adsorbate-adsorbent interactions on adsorption and suggests a uniform distribution of binding energies; and the energy of adsorption (Alkherraz et al., 2023; Elsherif et al., 2022; Matić et al., 2024).

Langmuir isotherm model: The Langmuir adsorption isotherm model was used to evaluate the adsorption behaviour of Methyl Green (MG) and Neutral Red (NR) dyes onto CMPF. Using the linear version of the Langmuir equation (equation 3), the slope and intercept of the plot of $1/Q_e$ vs 1/Ce (Figures 9A and 9B) were used to calculate the parameters Q_m (maximum adsorption capacity) and b (Langmuir constant). The correlation coefficient R^2 and the values of Q_m and b are shown in Table 3.

As demonstrated by the high correlation coefficients (R^2) of 0.9935 for NR dye and 0.9869 for MG dye, which show a strong alignment with the experimental data, the Langmuir model successfully characterises the adsorption process for both dyes. Indicating a greater contact between NR dye and the adsorbent surface, the Langmuir constant b, which measures the affinity between the adsorbent and the adsorbate, was higher for NR dye (0.730 L/mg) than for MG dye (0.513 L/mg). Furthermore, the Langmuir isotherm yielded maximum adsorption capacities (Q_m) of 19.88 mg/g for NR dye and 7.45 mg/g for MG dye, which closely matched the values of 14.5 mg/g and 9.5 mg/g, respectively, that were found experimentally. These results show that the observed adsorption behaviour and model predictions are consistent.

The dimensionless separation factor R_L, which is defined by the equation (Harouache et al., 2024), can be used to assess the favourability of the adsorption process because the experimental results closely matched the linear form of the Langmuir model:

$$R_L = \frac{1}{1 + bC_0} \tag{16}$$

The R_L values for both dyes ranged between 0 and 1, specifically from 0.07 to 0.13 for NR and from 0.21 to 0.33 for MG, indicating that the adsorption process was favorable under the studied experimental conditions.

Figure 9
Langmuir isotherm plot of NR (A) and MG (B) dyes onto CMPF

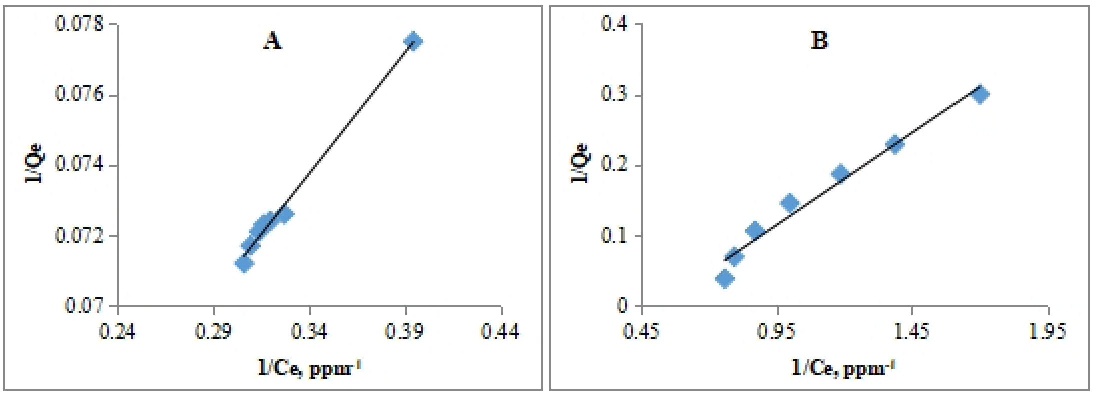

Freundlich isotherm model: The Freundlich isotherm characterises a physical adsorption process that occurs in several layers with comparatively weak connections, assuming heterogeneity of the adsorption sites (Matić et al., 2024). Equation 4 was used to get the Freundlich equilibrium constants from the linear plot of Log Q_e vs. Log C_e, which is displayed in Figure 10 (A & B). Even though it is empirical, the Freundlich isotherm provides valuable insights into the behaviour of adsorption, particularly in heterogeneous systems. The parameter n indicates the adsorption intensity; lower n values often suggest chemical adsorption rather than physical adsorption (Elsherif et al., 2024a). As shown in Table 3, the n values derived from the Freundlich equation were 3.995 for NR dye and 0.634 for MG dye. For NR dye adsorption, the n value of 3.995 indicates a mostly physical contact, but the n value of 0.634 for MG dye shows a potential chemical interaction. The high R^2 values show that the Freundlich model fits well the experimental data quite well (0.9965 for NR and 0.9698 for MG).

Figure 10
Freundlich isotherm plot of NR (A) and MG (B) dyes onto CMPF

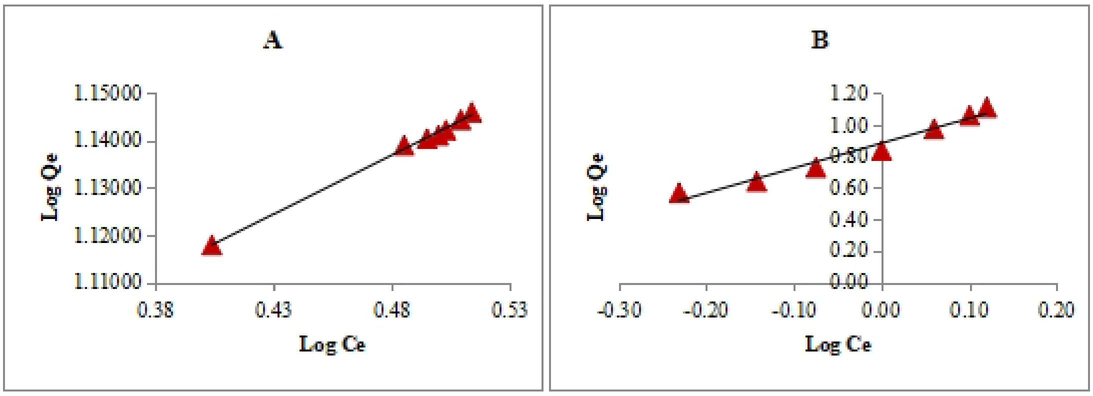

Temkin isotherm model: The Temkin isotherm states that the adsorption mechanism requires interactions between the adsorbent and adsorbate, the adsorption process assumes a uniform distribution of binding energy across the adsorbent surface, and the heat of adsorption decreases linearly as the adsorbent surface coverage increases (El-Shafie et al., 2023; Hammad et al., 2024). The isotherm constants (Figures 11A and 11B) obtained by plotting Q_e against Ln Ce are summarised as follows (Table 3): B_T = 2.127 and 17.14 J/mol (the heat of biosorption, which gives information on the energy changes during adsorption) and K_T = 215.8 and 1.804 L/mg (the equilibrium binding constant) for NR and MG dyes, respectively.

Stronger interactions between the adsorbent and adsorbate are indicated by a greater equilibrium binding constant (K_T), which is linked to the maximal binding energy (Olusegun et al., 2023; Rashid et al., 2021). Additionally, the Temkin isotherm model and the experimental results show a good agreement, as indicated by the correlation coefficients (R^2) of 0.7381 for MG and 0.9234 for NR.

Figure 11
Temkin isotherm plot of NR (A) and MG (B) dyes onto CMPF

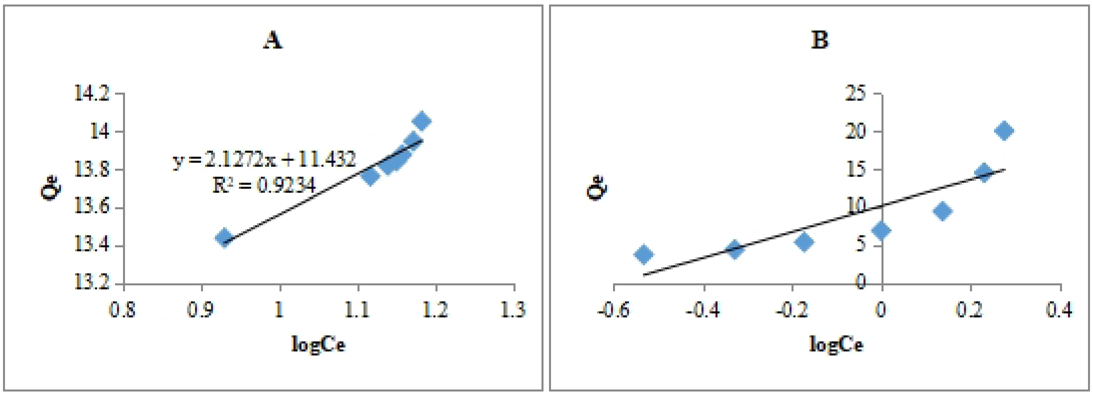

Dubinin-Radushkevich isotherm model: The Dubinin-Radushkevich (D-R) isotherm describes adsorption processes on adsorbents with heterogeneous surfaces or pore architectures and provides information on the free energy of adsorption. This theory states that micropore volume filling causes adsorption to occur (Elsherif et al., 2022; Memetova et al., 2023). Using the slope and intercept of the linear plots (Figures 12A and 12B), equations 6 and 7 were utilised to determine the D-R isotherm parameters, β and Q_m. An overview of the calculated values is given in Table 3. The experimental data and the D-R model showed a reasonable connection, with R^2 values of 0.9874 for NR dye and 0.8363 for MG dye.

Using Equation 17, the free energy of adsorption (E) per adsorbate molecule was calculated (Alkherraz et al., 2023):

$$E = \frac{1}{\sqrt{2k}} \tag{17}$$

The energy required to extract a molecule from the surface is reflected in this energy. Physical adsorption ($E < 8$ kJ/mol) and chemical adsorption ($8 < E < 168$ kJ/mol) are distinguished by the equation. For NR dye, the values of E were 0.500 kJ/mol, while for MG dye, they were 0.408 kJ/mol. These findings demonstrate that both colours biosorption onto CMPF powder is essentially a physical adsorption process.

Figure 12
Dubinin-Radushkevich isotherm plot of NR (A) and MG (B) dyes onto CMPF

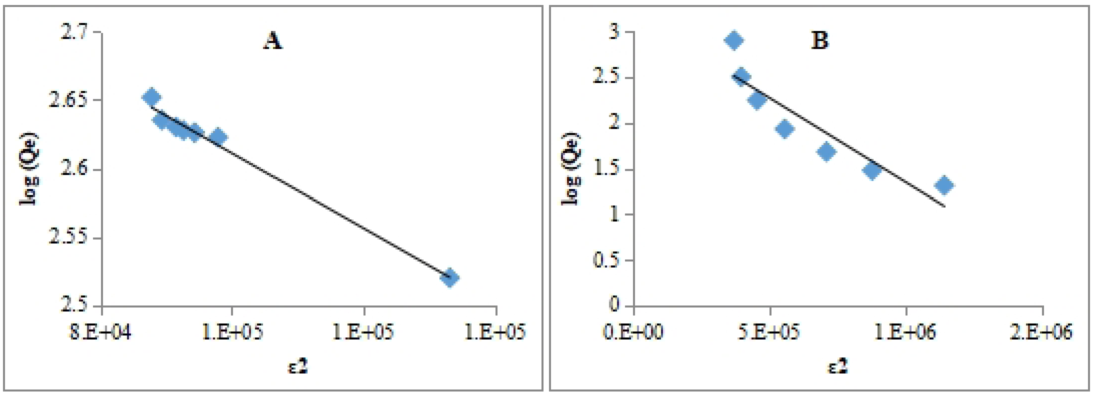

Table 3

Several isotherm models parameters for NR and MG adsorption onto CMPF

Model	Parameter	Value	
		NR	MG
Langmuir	b (L/mg)	0.730	0.513
	Q_m (mg/g)	19.88	7.452
	R^2	0.9935	0.9724
Freundlich	K_F (mg/g (L/mg)$^{1/n}$)	10.39	7.642
	n	3.995	0.634
	R^2	0.9965	0.9698
Temkin	B_T (J/mol)	2.127	17.14
	K_T (L/mg)	215.8	1.804
	R^2	0.9234	0.7381
Dubinin-Radushkevich	Q_m (mg/g)	17.64	24.25
	β (mol²/J²)	3x10^{-6}	2x10^{-6}
	E (kJ/mol)	0.408	0.500
	R^2	0.9874	0.8363

Comparison of Adsorption Performance and Mechanisms: The adsorption behavior of functionalized palm fibers (CMPF) for neutral red (NR) and methyl green (MG) aligns with trends observed in recent studies on dye removal using sustainable adsorbents. For NR, the Langmuir maximum adsorption capacity (Q_m = 19.88 mg/g) surpasses values reported for manganese-bismuth oxide composites (Q_m = 1.4 mg/g) (Al-Saeedi et al., 2023) and raw olive stone (Q_m = 4.5 mg/g) (Alardhi et al., 2023), though it is lower than high-performance materials like magnetite-supported avocado stone biochar (Q_m = 118.9 mg/g) (El-Shafie et al., 2023) or peanut shell activated carbon (Q_m = 109.89 mg/g) (Sanou et al., 2024). This positions CMPF as a competitive alternative for moderate-concentration dye removal, particularly given its reliance on low-energy chemical functionalization compared to energy-intensive activated carbon synthesis (Fito et al., 2023; Sanou et al., 2024). For MG, the lower Q_m (7.45 mg/g) may stem from electrostatic or steric mismatches, but contrasts with the high efficiency of magnetite-modified composites (El-Shafie et al., 2023), highlighting the need for tailored adsorbent-dye pairing.

The Freundlich model's dominance for NR (R^2 = 0.9965, n = 3.995) suggests heterogeneous multilayer adsorption, similar to findings for Congo Red on sugarcane bagasse (Elsherif et al., 2017) and MB on *Rumex abyssinicus* activated carbon (R^2 = 0.99 for Freundlich) (Fito et al., 2023). In contrast, MG's stronger alignment with the Langmuir model (R^2 = 0.9724) reflects monolayer adsorption trends observed for MB on olive stone (Alardhi et al., 2023) and cellulose-$Fe_{33}O_{44}$ (Pietrzyk et al., 2023). The low Dubinin-Radushkevich (D-R) mean free energy (E < 0.5 kJ/mol) confirms physical adsorption for both dyes, consistent with studies on rice husk (Alshorifi et al., 2022) and peanut shells (Sanou et al., 2024), but diverges from chemisorption mechanisms reported for Mn_3O_4-Bi_2O_3 composites (Al-Saeedi et al., 2023) and tella residue biosorbents (Abate et al., 2023).

Notably, CMPF achieves these results without the need for magnetic nanoparticle integration (El-Shafie et al., 2023; Pietrzyk et al., 2023) or extreme pH conditions (e.g., pH 9 for *Rumex abyssinicus* (Fito et al., 2023)), emphasizing its simplicity and scalability. While its adsorption capacity is lower than activated carbons (Sanou et al., 2024), its sustainability metrics – avoiding pyrolysis (e.g., 500°C for coconut husk biochar (Minh et al., 2023)) and utilizing palm fiber waste – align with circular economy principles, as advocated in studies on olive stone (Alardhi et al., 2023) and avocado stone biochar (El-Shafie et al., 2023).

Adsorption kinetic models: Adsorption kinetics examination is necessary to comprehend the adsorption process, including its pace and the principles underlying mass transfer. For effective adsorption system scaling up and system design optimisation, this information is essential (Minh et al., 2023; Qureshi et al., 2020). Kinetic assessments can also be used to determine the adsorbent's saturation time (Ahmed & Hameed, 2019; Qureshi et al., 2020). In adsorption studies, the pseudo-first-order (PFO), pseudo-second-order (PSO), Elovich, and intraparticle diffusion models are often employed kinetic models.

Pseudo first-order model: To utilise the integrated form of the pseudo-first-order kinetic model (Equation 8), the equilibrium sorption capacity, Q_e, must be determined. Therefore, it is often required to estimate Q_e by a trial-and-error approach in order to assess the model's kinetics. The plots for pseudo-first order are displayed in Figures 13A and 13B. The calculated parameters and the linear regression correlation coefficients (R^2) are shown in Table 4. For NR and MG dyes, the corresponding R^2 values of 0.7833 and 0.7862 indicate a reasonable but not very strong fit. This suggests that the experimental data may be better represented by alternative kinetic models. Additionally, as Table 4 illustrates, the computed sorption capacities (Q_e) do not match the experimentally determined values.

Figure 13

Pseudo first-order plot of NR (A) and MG (B) dyes onto CMPF

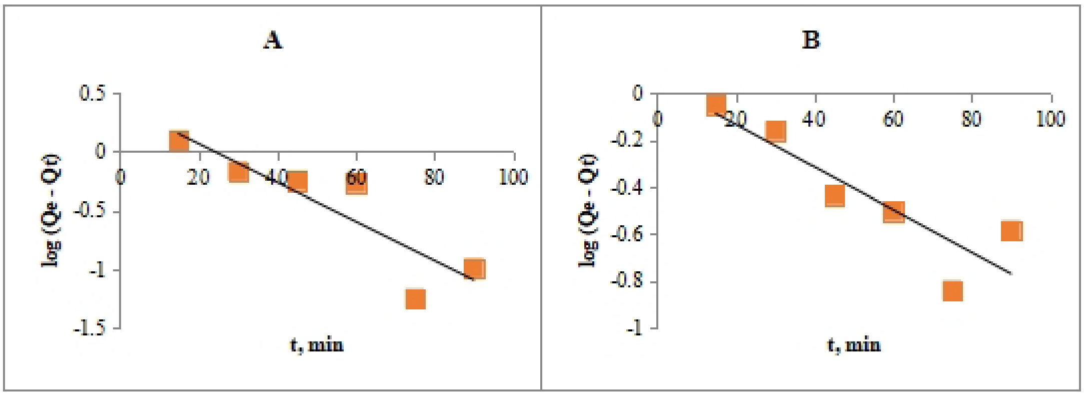

Pseudo second-order model: The plot of t/Q_t vs. t should show a linear relationship according to Equation 9, enabling it possible to determine Q_e and k_2 from the slope and intercept of the plot (Figures 14A and 14B). The calculated Q_e values, the pseudo-second-order rate constant (k_2), and the corresponding linear regression correlation coefficients (R^2) are summarised in Table 4. The correlation coefficients for the pseudo-second-order model were significantly higher than those for the pseudo-first-order model for NR and MG dyes, at 0.9988 and 0.9989, respectively. This indicates that the pseudo-second-order kinetic model provides a more accurate representation of the adsorption data.

The pseudo-second-order model states that the adsorption rate is determined by the square of the number of unoccupied sites (El-Hashani et al., 2018b). Furthermore, the high agreement between the estimated and empirically determined Q_e values further supports the usefulness of this model in understanding the adsorption process. These findings suggest that the adsorption of NR and MG dyes onto the adsorbent is most likely caused by chemisorption, which entails electron sharing or exchange between the adsorbent and the adsorbate.

Figure 14

Pseudo second-order plot of NR (A) and MG (B) dyes onto CMPF

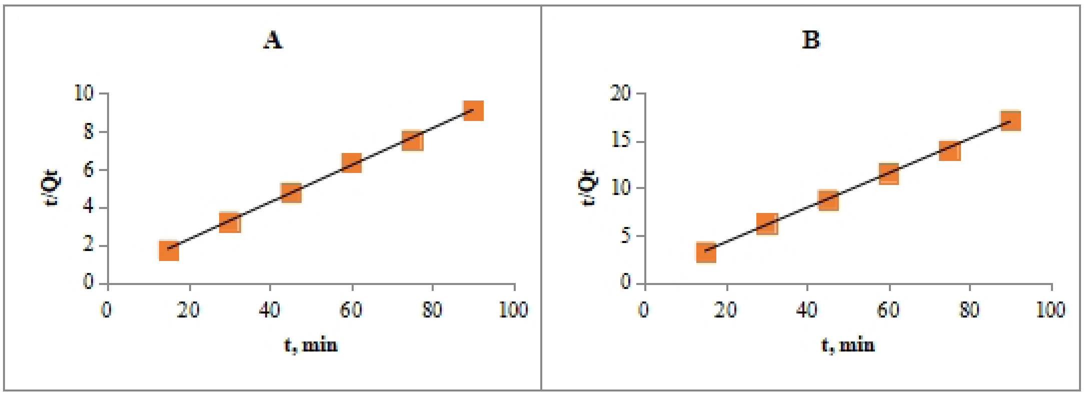

Intra-particle diffusion model: If intraparticle diffusion has a major impact on the adsorption process, a plot of Q_t vs $t^{1/2}$ should have a linear connection, as per the intraparticle diffusion hypothesis. Intraparticle diffusion is the only rate-controlling step if the resulting lines cross at the origin. On the other hand, it indicates that boundary layer control is also in operation and that the adsorption rate is being influenced by other mechanisms if the lines do not cross through the origin. This suggests that several processes may be taking place at the same time and that intraparticle diffusion is not the only rate-controlling mechanism (Ahmed & Hameed, 2019; Si et al., 2015).

Equation 10 may be used to calculate the values of C_e (boundary layer thickness) and K_d (intraparticle diffusion rate constant) from the slope and intercept of the plot of Q_t versus $t^{1/2}$, as illustrated in Figures 15A and 15B. The lines' apparent departure from the origin demonstrates that the adsorption process is not only governed by intraparticle diffusion.

According to this result, the biosorption of NR and MG dyes onto CMPF powder is a complicated process that includes both surface biosorption and intraparticle diffusion as rate-limiting factors. The correlation coefficient values in Table 4 demonstrate that, in spite of this complexity, the model suited the experimental data very well.

Figure 15
Intra-particle diffusion plot of NR (A) and MG (B) dyes onto CMPF

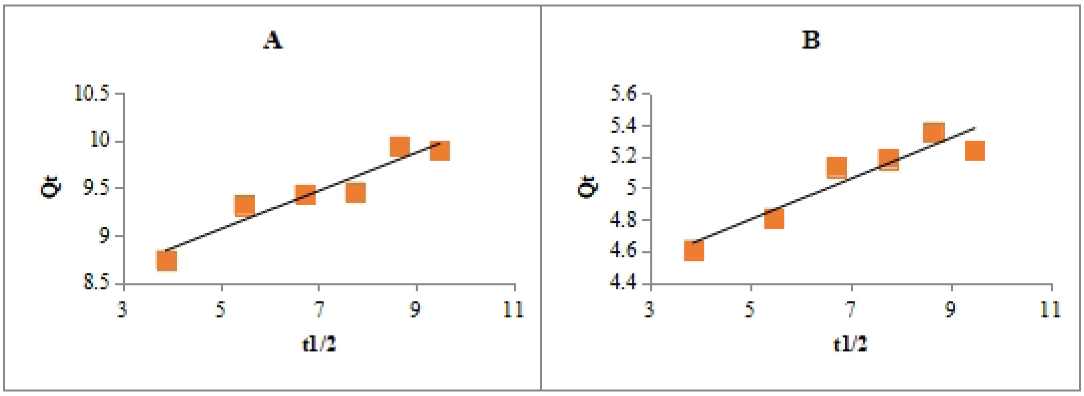

Elovich model: The adsorption of dissolved compounds from liquid solutions has been successfully represented using the Elovich equation, which was first created for chemical kinetics. Based on the slope and intercept of the Ln Q_t vs. Ln t plot (Figures 16A and 16B), Equation 11 was utilised to determine the Elovich parameters β (surface coverage-related desorption constant) and α (initial adsorption rate). The resulting results are summarised in Table 4, which gives β values for NR and MG dyes of 0.682 and 1.050 g/mg and α values of 93,100 and 21,800 mg/g.min.

The experimental data fits the Elovich model rather well, as indicated by the correlation coefficients (R^2) of 0.8894 for MG dye and 0.9109 for NR dye. This implies that, under the specified experimental conditions, the Elovich equation offers a satisfactory explanation of the adsorption kinetics for the dyes under study.

Figure 16
Elovich plot of NR (A) and MG (B) dyes onto CMPF

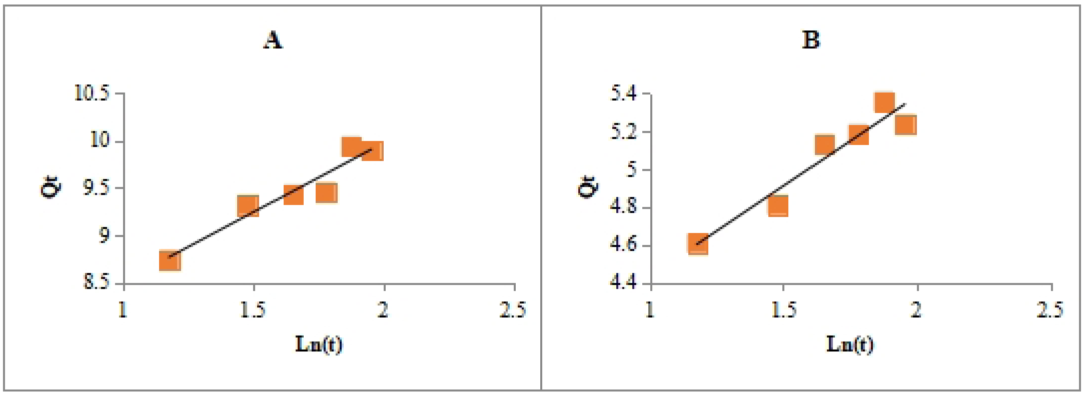

Table 4
Kinetic model parameters for NR and MG adsorption onto CMPF

Pseudo-first-order	k_1 (min^{-1})	Q_e (Cal.) (mg/g)	Q_e (Exp.) (mg/g)	R^2
NR	0.0382	2.52	10.00	0.7833
MG	0.0210	1.12	5.50	0.7862
Pseudo-second-order	k_2 ($g.mg^{-1}.min^{-1}$)	Q_e (Cal.) (mg/g)	Q_e (Exp.) (mg/g)	R^2
NR	0.0315	10.20	10.00	0.9988
MG	0.0559	5.48	5.50	0.9989
Elovich	β ($g.mg^{-1}$)	α ($mg.g^{-1}.min^{-1}$)	R^2	
NR	0.682	$9.31x10^4$	0.9232	
MG	1.050	$2.18x10^4$	0.9243	
Intra-particle diffusion	K_d ($mg.g^{-1}.min^{-1}$)	C_e (mg/g)	Q_e (Exp.) (mg/g)	R^2
NR	0.2013	8.06	10.00	0.9109
MG	0.1292	4.15	5.50	0.8894

Adsorption thermodynamics: To ascertain the spontaneity of a biosorption process, thermodynamic analysis is necessary. The Gibbs free energy change (ΔG), a crucial metric in determining whether a process happens spontaneously, can be calculated using the standard Van't Hoff equation (Equation 15). The enthalpy change (ΔH) and entropy change (ΔS) were determined using the slope and intercept of the Ln K_d against 1/T plot. Equation 12 was then utilised to compute the Gibbs free energy change for sorption.

The thermodynamic behaviour of NR and MG dye adsorption on CMPF was assessed by experiments conducted at different temperatures. The temperature-dependent adsorption efficiency of NR and MG dyes is depicted in Figures 8A and 8B. The slope and intercept of a linear plot of Ln K_d versus 1/T are shown in Figures 17A and 17B, and these were utilised to get the values of ΔH˚ and ΔS˚. Throughout the studied temperature range, a spontaneous adsorption process is demonstrated by the negative ΔG values at all temperatures. The adsorption process is endothermic and involves heat absorption, as indicated by the positive ΔH° values (12.783 and 8.662 kJ/mol).

The high affinity of the dye molecules for CMPF is further demonstrated by the positive ΔS° values (68.49 and 68.12 J/mol.K), which show enhanced disorder at the solid-liquid interface during adsorption. The negative ΔG° results further support the process' spontaneity. The combined results of ΔS° and ΔG° show that the reaction is thermodynamically favourable and proceeds spontaneously as a result of an increase in entropy.

Figure 17
Van't Hoff plot of NR (A) and MG (B) dyes onto CMPF

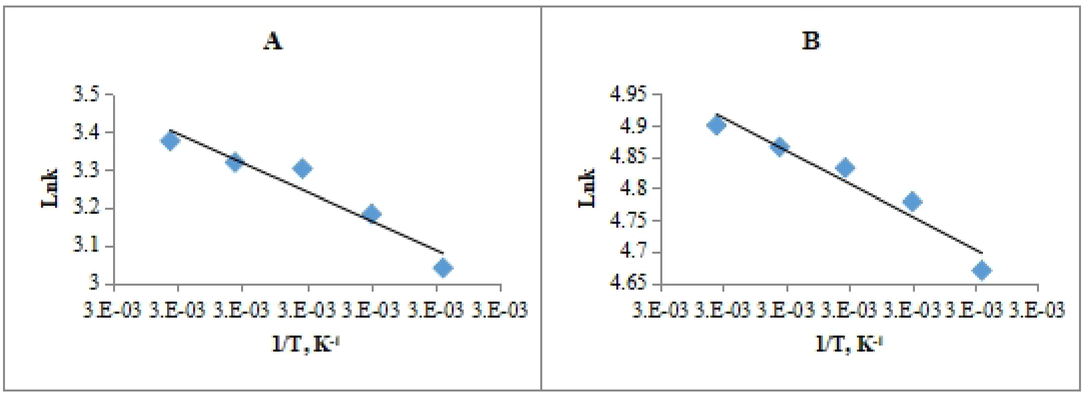

Table 5
Thermodynamic parameters for the adsorption of dyes onto CMPF

Dye	Temperature (K)	ΔG (kJ/mol)	ΔH^0 (kJ/mol)	ΔS^0 (J/mol. k)	R^2
NR	298	-7.637	12.783	68.49	0.9191
	303	-7.980			
	308	-8.322			
	313	-8.665			
	318	-9.007			
MG	298	-11.648	8.662	68.12	0.9357
	303	-11.989			
	308	-12.329			
	313	-12.670			
	318	-13.010			

Conclusion

This study examined two palm fibre-derived adsorbents: chemically modified palm fibre using carbon disulphide (CMPF) and acid-base treated palm fibre (A-BTPF), for dye removal from water. The results consistently demonstrated that CMPF exhibited superior adsorption capacity and efficiency compared to A-BTPF under all experimental conditions. The enhanced performance of CMPF, achieved through chemical modification with CS_2, introduced functional groups such as aldehydes and xanthates, significantly increasing its dye adsorption potential. FT-IR analysis confirmed the structural modifications caused by the chemical treatments.

pH investigations revealed that both adsorbents showed maximum removal efficiencies for neutral red (NR) at pH 4 and for methylene green (MG) at pH 10 (72% for CMPF and 61% for A-BTPF), indicating pH-dependent adsorption. The Langmuir isotherm model provided the best fit for the adsorption data, with maximum adsorption capacities of 19.88 mg/g for NR and 7.45 mg/g for MG, and high R^2 values of 0.9935 and 0.9869, respectively. Kinetic studies further confirmed that the adsorption process followed a pseudo-second-order model, with strong correlation coefficients of 0.9988 for NR and 0.9989 for MG.

Thermodynamic analysis indicated that the adsorption process is spontaneous and endothermic, driven by increased entropy, as evidenced by positive ΔH°, ΔS° values and negative ΔG° values across all temperatures. These findings underscore the potential of CMPF as an effective, sustainable biosorbent for dye removal, with its chemical modification offering enhanced adsorption properties compared to conventional treatments.

Authors contribution

A. El-Hashani: Conceptualization, Investigation, Methodology, Writing – original draft. K.M. Elsherif: Conceptualization, Methodology, Supervision, Funding acquisition, Resources, Writing – review & editing. G.F. Musbah: Investigation, Data curation, Formal analysis, Validation. A. Imragaa: Investigation, Resources, Software, Visualization. H.F. Emrayed: Formal analysis, Validation, Writing – review & editing.

Acknowledgement

We would like to deeply appreciate the University of Benghazi's Department of Chemistry, Faculty of Science, for all of their help and resources during this project. Their dedication to establishing an innovative and cooperative research atmosphere was crucial to this study's success.

Conflict of interest

The authors declare that they have no conflicts of interest.

References

1. Abate, G. Y., Nguyen, D. T. A., Alene, A. N., Kassie, D. A., Addiss, Y. A., & Mintesinot, S. M. (2023). Cereal based traditional beverage of tella residue (attela) as a green organic pollutant sorbent for methylene blue dye removal: Equilibrium, kinetics and thermodynamic studies. *Indian Journal of Chemical Technology, 30*(2), 151–164. https://doi.org/10.56042/ijct.v30i2.64532

2. Abuzerr, S., Darwish, M., & Mahvi, A. H. (2018). Simultaneous removal of cationic methylene blue and anionic reactive red 198 dyes using magnetic activated carbon nanoparticles: Equilibrium, and kinetics analysis. *Water Science and Technology, 2017*(2), 534–545. https://doi.org/10.2166/wst.2018.145

3. Ahmed, M. J., & Hameed, B. H. (2019). Insights into the isotherm and kinetic models for the coadsorption of pharmaceuticals in the absence and presence of metal ions: A review. *Journal of Environmental Management, 252*, Article 109617. https://doi.org/10.1016/j.jenvman.2019.109617

4. Alardhi, S. M., Salih, H. G., Ali, N. S., Khalbas, A. H., Salih, I. K., Cata Saady, N. M., Zendehboudi, S., Albayati, T. M., & Harharah, H. N. (2023). Olive stone as an eco-friendly bio-adsorbent for elimination of methylene blue dye from industrial wastewater. *Scientific Reports, 13*(1), Article 21063. https://doi.org/10.1038/s41598-023-47319-x

5. Alkherraz, A. M., Ali, A. K., & Elsherif, K. M. (2020a). Equilibrium and thermodynamic studies of Pb(II), Zn(II), Cu(II) and Cd(II) adsorption onto Mesembryanthemum activated carbon. *Journal of Medicinal Chemical Sciences, 3*(1), 1–10. https://doi.org/10.33945/SAMI/JMCS.2020.1.1

6. Alkherraz, A. M., Ali, A. K., & Elsherif, K. M. (2020b). Removal of Pb(II), Zn(II), Cu(II) and Cd(II) from aqueous solutions by adsorption onto olive branches activated carbon: Equilibrium and thermodynamic studies. *Chemistry International, 6*(1), 11–20.

7. Alkherraz, A. M., Elsherif, K. M., & Blayblo, N. A. (2023). Safranin adsorption onto Acasia plant-derived activated carbon: Isotherms, thermodynamics, and kinetic studies. *Chemistry International, 9*(4), 134–145. https://doi.org/10.5281/zenodo.812768

8. Alkherraz, A. M., Elsherif, K. M., El-Dali, A., Blayblo, N. A., & Sasi, M. (2022). Thermodynamic, equilibrium, and kinetic studies of safranin adsorption onto Carpobrotus edulis. *Asian Journal of Nanoscience and Materials, 5*(2), 118–131. https://doi.org/10.26655/ajnanomat.2022.2.4

9. Al-Saeedi, S. I., Areej, A., Qamar, M. T., Alhujaily, A., Iqbal, S., Alotaibi, M. T., Aslam, M., Qayyum, M. A., Bahadur, A., Awwad, N. S., Jazaa, Y., & Elkaeed, E. B. (2023). Isotherm and kinetic studies for the adsorption of methylene blue onto a novel Mn_3O_4–Bi_2O_3 composite and their antifungal performance. *Frontiers in Environmental Science, 11*, Article 1156475. https://doi.org/10.3389/fenvs.2023.1156475

10. Alshorifi, F. T., Ali, S. L., & Salama, R. S. (2022). Promotional synergistic effect of Cs–Au NPs on the performance of Cs–Au/$MgFe_2O_4$ catalysts in the catalysis of 3,4-dihydropyrimidin-2(1H)-ones and degradation of RhB dye. *Journal of Inorganic and Organometallic Polymers and Materials, 32*(10), 3765–3776. https://doi.org/10.1007/s10904-022-02389-8

11. Alver, E., Metin, A. Ü., & Brouers, F. (2020). Methylene blue adsorption on magnetic alginate/rice husk bio-composite. *International Journal of Biological Macromolecules, 154*, 104–113. https://doi.org/10.1016/j.ijbiomac.2020.02.330

12. Ansari, R., & Mosayebzadeh, Z. (2010). Removal of Basic Dye Methylene Blue from aqueous solutions using sawdust and sawdust coated with polypyrrole. *Journal of the Iranian Chemical Society, 7*(2), 339–350. https://doi.org/10.1007/BF03246019

13. Belgacem, A., Ould Brahim, I., Belmedani, M., & Hadoun, H. (2022). Removal of methyl green dye from aqueous solutions using activated carbon derived from cryogenic crushed waste tires. *Iranian Journal of Chemistry and Chemical Engineering, 41*(1), 207–219. https://doi.org/10.30492/ijcce.2020.121562.3966

14. Ben-Ali, S., Jaouali, I., Souissi-Najar, S., & Ouederni, A. (2017). Characterization and adsorption capacity of raw pomegranate peel biosorbent for copper removal. *Journal of Cleaner Production, 142*(4), 3809–3821. https://doi.org/10.1016/j.jclepro.2016.10.081

15. Bibikov, S. B., Sergeev, A. I., Barashkova, I. I., Isaykina, N. V., Gusev, A. A., & Semenov, A. N. (2024). The combined effects of electrochemical and ultrasonic treatment for water purification from pathogenic contaminants based on the example of Escherichia coli. *Biophysics, 69*(2), 272–277. https://doi.org/10.1134/S0006350924700325

16. Budi, A., Stipp, S. L. S., & Andersson, M. P. (2018). The effect of solvation and temperature on the adsorption of small organic molecules on calcite. *Physical Chemistry Chemical Physics, 20*(10), 7140–7147. https://doi.org/10.1039/c7cp06747j

17. Caldeira, A. S., Fabris, J. D., Nelson, D. L., & Damasceno, S. M. (2018). Removal of textile dye by adsorption on the cake as solid waste from the press-extraction of the macaúba (Acrocomia aculeata) kernel oil. *Eclética Química Journal, 43*(1), 48–53. https://doi.org/10.26850/1678-4618eqj.v43.1.48-53

18. Devi, R., Kumar, V., Kumar, S., Sharma, K., & Kumar, R. (2023). Recent advancement in biomass-derived activated carbon for wastewater treatment, energy storage, and gas purification: A review. *Journal of Materials Science, 58*(29), 12119–12142. https://doi.org/10.1007/s10853-023-08773-0

19. Din, H., Kiran, M., Haq, F., Osman, A. I., Khan, I. A., Aziz, T., Khan, A., & Jilani, S. (2024). Synergizing date palm seeds-derived oxidized activated carbon: Sustainable innovation for enhanced water retention, efficient wastewater treatment, and synthetic dye removal. *Chemical Engineering Research and Design, 204*, 212–227. https://doi.org/10.1016/j.cherd.2024.02.040

20. Djama, C., Bouguettoucha, A., Chebli, D., Amrane, A., Tahraoui, H., Zhang, J., & Mouni, L. (2023). Experimental and theoretical study of methylene blue adsorption on a new raw material, Cynara scolymus—A statistical physics assessment. *Sustainability, 15*(13), Article 10364. https://doi.org/10.3390/su151310364

21. Dural, M. U., Cavas, L., Papageorgiou, S. K., & Katsaros, F. K. (2011). Methylene blue adsorption on activated carbon prepared from Posidonia oceanica (L.) dead leaves: Kinetics and equilibrium studies. *Chemical Engineering Journal, 168*(1), 77–85. https://doi.org/10.1016/j.cej.2010.12.038

22. El-Hashani, A., Ben Khayal, N., & Elsherif, K. M. (2018a). Selective transport of aromatic compounds across parchment-supported Prussian blue membrane. *Chemical Methodologies, 2*(3), 194–203. https://doi.org/10.22631/chemm.2018.118847.1038

23. El-Hashani, A., Elsherif, K. M., Edbey, K., Alfaqih, F., Alomammy, M., & Alomammy, S. (2018b). Biosorption of Eriochrome Black T (EBT) onto waste tea powder: Equilibrium and kinetic studies. *Total Chemistry, 1*(3), 263–275.

24. Elsherif, K. M., Alkherraz, A. M., Edwards, H., & Mutawia, B. Y. A. (2024a). Congo red dye adsorption on dry green pea husk: Effects of process parameters and modeling approaches. *Environmental Health Engineering and Management Journal, 11*(3), 273–284. https://doi.org/10.34172/EHEM.2024.27

25. Elsherif, K. M., Alkherraz, A. M., Madri, A. H., Eldali, A., & Yaghi, M. M. (2024b). Kinetic, isotherm, and thermodynamic modeling of methylene blue adsorption by hibiscus plant waste derived biosorbents. *Journal of Chemical Health Risks, 14*(4), 727–740. https://doi.org/10.60829/jchr.2024.1977

26. Elsherif, K. M., El-Dali, A., Ewlad-Ahmed, A. M., Treban, A., & Alttayib, I. (2021). Removal of safranin dye from aqueous solution by adsorption onto olive leaves powder. *Journal of Materials and Environmental Science, 12*(3), 418–430.

27. Elsherif, K. M., El-Dali, A., Ewlad-Ahmed, A. M., Treban, A., Alqadhi, H., & Alkarewi, S. (2022). Kinetics and isotherms studies of safranin adsorption onto two surfaces prepared from orange peels. *Moroccan Journal of Chemistry, 10*(4), 639–651. https://doi.org/10.48317/IMIST.PRSM/morjchem-v11i1.32137

28. Elsherif, K. M., El-Hashani, A., & Haider, I. (2018a). Biosorption of Fe(III) onto coffee and tea powder: Equilibrium and kinetic study. *Asian Journal of Green Chemistry, 2*(4), 380–394. https://doi.org/10.22034/ajgc.2018.65163

29. Elsherif, K. M., El-Hashani, A., & Haider, I. (2018b). Equilibrium and kinetic studies of Cu(II) biosorption onto waste tea and coffee powder (WTCP). *Iranian Journal of Analytical Chemistry, 5*(2), 31–38. https://doi.org/20.1001.1.23832207.2018.5.2.5.4

30. Elsherif, K. M., El-Hashani, A., El-Dali, A., & Saad, M. (2014a). Ion-permeation rate of (1:1) electrolytes across parchment-supported silver chloride membrane. International *Journal of Chemical and Pharmaceutical Sciences, 2*(6), 890–897.

31. Elsherif, K. M., El-Hashani, A., El-Dali, A., & Musa, M. (2014b). Ion selectivity across parchment-supported silver chloride membrane in contact with multi-valent electrolytes. *International Journal of Analytical and Bioanalytical Chemistry, 4*(2), 58–62.

32. Elsherif, K. M., Ewlad-Ahmed, A. M., & Treban, A. (2017). Removal of Fe(III), Cu(II), and Co(II) from aqueous solutions by orange peels powder: Equilibrium study. *World Journal of Biochemistry and Molecular Biology, 2*(6), 46–51.

33. Elsherif, K. M., Haider, I., & El-Hashani, A. (2019). Adsorption of Co (II) ions from aqueous solution onto tea and coffee powder: Equilibrium and kinetic studies. *Journal of Fundamental and Applied Sciences, 11*(1), 65–81. https://doi.org/10.4314/jfas.v11i1.5

34. Elsherif, K. M., & Yaghi, M. M. (2017). Studies with model membrane: The effect of temperature on membrane potential. *Moroccan Journal of Chemistry, 5*(1), 131–138. https://doi.org/10.48317/IMIST.PRSM/morjchem-v5i1.6324

35. El-Shafie, A. S., Karamshahi, F., & El-Azazy, M. (2023). Turning waste avocado stones and montmorillonite into magnetite-supported nanocomposites for the depollution of methylene blue: Adsorbent reusability and performance optimization. *Environmental Science and Pollution Research, 30*(50), 118764–118781. https://doi.org/10.1007/s11356-023-30538-0

36. Fito, J., Abewaa, M., Mengistu, A., Angassa, K., Ambaye, A. D., Moyo, W., & Nkambule, T. (2023). Adsorption of methylene blue from textile industrial wastewater using activated carbon developed from Rumex abyssinicus plant. *Scientific Reports, 13*(1), Article 5427. https://doi.org/10.1038/s41598-023-32341-w

37. Geddeda, Y. I., & Abdassalam, F. (2010). Some physical characteristics of several Libyan date palm cultivars. *Acta Horticulturae, 882*, 733–736. https://doi.org/10.17660/ActaHortic.2010.882.80

38. Gutiérrez, M., Grillini, V., Mutavdžić Pavlović, D., & Verlicchi, P. (2021). Activated carbon coupled with advanced biological wastewater treatment: A review of the enhancement in micropollutant removal. *Science of The Total Environment, 790*, Article 148050. https://doi.org/10.1016/j.scitotenv.2021.148050

39. Hamedi, H., Zendehboudi, S., Rezaei, N., Azizi, A., & Shahhoseini, F. (2023). Application of functionalized Fe_3O_4 magnetic nanoparticles using CTAB and SDS for oil separation from oil-in-water nanoemulsions. *Langmuir, 39*(23), 7995–8007. https://doi.org/10.1021/acs.langmuir.2c03266

40. Hammad, W. A., Darweesh, M. A., Zouli, N., El-Metwaly, N. M., Ahmed, M. A., & El-Khateeb, A. Y. (2024). Adsorption of cationic dye onto Raphanus seeds: Optimization, adsorption kinetics, thermodynamic studies. *Scientific Reports, 14*(1), Article 17827. https://doi.org/10.1038/s41598-024-66761-z

41. Harouache, A., Kharroubi, M., Lefkaier, I. K., Harfouche, N., Attou, M., & Mouni, L. (2024). Adsorption of anionic dye onto homoionic montmorillonite: Effect of the exchangeable cation on the adsorption. *Journal of the Iranian Chemical Society, 21*(7), 1423–1438. https://doi.org/10.1007/s13738-024-03009-7

42. Homagai, P. L., Ghimire, K. N., & Inoue, K. (2010). Adsorption behavior of heavy metals onto chemically modified sugarcane bagasse. *Bioresource Technology, 101*(6), 2067–2069. https://doi.org/10.1016/j.biortech.2009.11.073

43. Huang, J., Ran, X., Sun, L., Bi, H., & Wu, X. (2024). Recent advances in membrane technologies applied in oil–water separation. *Discover Nano, 19*(1), Article 66. https://doi.org/10.1186/s11671-024-04012-w

44. Ibrahim, A. A., Salama, R. S., El-Hakam, S. A., Khder, A. S., & Ahmed, A. I. (2021). Synthesis of 12-tungstophosphoric acid supported on Zr/MCM-41 composite with excellent heterogeneous catalyst and promising adsorbent of methylene blue. *Colloids and Surfaces A: Physicochemical and Engineering Aspects, 631*, Article 127753. https://doi.org/10.1016/j.colsurfa.2021.127753

45. Islam, N. A. B. M., Kayo, N., Motoishi, Y., Yoshimatsu, I., Yoshitomi, S., Seo, A., & Kuroda, S. (2024). Kinetics and thermodynamics analysis of the polybenzimidazole adsorption onto carbon materials using adsorption isotherm measurements. *Polymer Journal, 56*, 1153–1163. https://doi.org/10.1038/s41428-024-00950-5

46. Lakshmi, D. S., Ravindran, L., Mary, P. J. M., George, T., Muthusamy, S., & Sukumar, M. (2024). Valorization of crustacean shells: Preparation, characterization, and chemical modification of nano-chitin biopolymer membrane for application in water purification. *Waste and Biomass Valorization, 15*(10), 6067–6090. https://doi.org/10.1007/s12649-024-02601-5

47. Li, A., Gong, Y., Zhao, D., Dang, A., & Lin, Z. (2021). Enhanced removal of zinc and cadmium from water using carboxymethyl cellulose-bridged chlorapatite nanoparticles. *Chemosphere, 263*, Article 128038. https://doi.org/10.1016/j.chemosphere.2020.128038

48. Madadgar, S., Doulati Ardejani, F., Boroumand, Z., Sadeghpour, H., Taherdangkoo, R., & Butscher, C. (2023). Biosorption of aqueous Pb(II), Co(II), Cd(II) and Ni(II) ions from Sungun Copper Mine wastewater by Chrysopogon zizanioides root powder. *Minerals, 13*(1), Article 106. https://doi.org/10.3390/min13010106

49. Matić, P., Ukić, Š., & Jakobek, L. (2024). Adsorption of procyanidins B1 and B2 onto β-Glucan: Adsorption isotherms and thermodynamics. *Adsorption, 30*(7), 1303–1313. https://doi.org/10.1007/s10450-024-00503-5

50. Melliti, A., Srivastava, V., Kheriji, J., Sillanpää, M., & Hamrouni, B. (2021). Date palm fiber as a novel precursor for porous activated carbon: Optimization, characterization and its application as Tylosin antibiotic scavenger from aqueous solution. *Surfaces and Interfaces, 24*, Article 101047. https://doi.org/10.1016/j.surfin.2021.101047

51. Memetova, A. E., Zelenin, A. D., Memetov, N. R., Tkachev, A. G., & Memetov, R. E. (2023). Methane adsorption properties of a functional porous material based on coffee waste. *Inorganic Materials: Applied Research, 14*(5), 1298–1304. https://doi.org/10.1134/S2075113323050295

52. Minh, V. C., Lien, N. T. L., Thuy, N. T., Phung, L. T. K., & Huy, N. N. (2023). Production of biochar from coconut husks for adsorption of heavy metals in water. *Philippine Journal of Science, 152*(5), 1579–1593. https://doi.org/10.56899/152.05.05

53. Nasiri, M., Ahmadzadeh, H., & Amiri, A. H. (2023). Biodegradation and metabolic fate of organophosphorus pesticides in well water using Dunaliella salina. *International Journal Environmental Science and Technology, 20*(1), 981–992. https://doi.org/10.1007/s13762-022-04620-y

54. Olusegun, S. J., Osial, M., Souza, T. G. Z., Krajewski, M., Rodrigues, G. L. S., Pękała, M., & Krysinski, P. (2023). Comparative characteristics and enhanced removal of tetracycline and ceftriaxone by Fe_3O_4-lignin and Fe_3O_4-carbon-based lignin: Mechanism, thermodynamic evaluation, and DFT calculation. *Journal of Molecular Liquids, 371*, Article 21075. https://doi.org/10.1016/j.molliq.2022.121075

55. Pathania, D., Sharma, S., & Singh, P. (2017). Removal of methylene blue by adsorption onto activated carbon developed from Ficus carica bast. *Arabian Journal of Chemistry, 10*(Suppl. 1), S1445–S1451. https://doi.org/10.1016/j.arabjc.2013.04.021

56. Pietrzyk, P., Borowska, E. I., Hejduk, P., Camargo, B. C., Warczak, M., Nguyen, T. P., Pregowska, A., Gniadek, M., Szczytko, J., & Wilczewski, S. (2023). Green composites based on volcanic red algae Cyanidiales, cellulose, and coffee waste biomass modified with magnetic nanoparticles for the removal of methylene blue. *Environmental Science and Pollution Research, 30*(23), 62689–62703. https://doi.org/10.1007/s11356-023-26425-3

57. Qureshi, U. A., Hameed, B. H., & Ahmed, M. J. (2020). Adsorption of endocrine disrupting compounds and other emerging contaminants using lignocellulosic biomass-derived porous carbons: A review. *Journal of Water Process Engineering, 38*, Article 101380. https://doi.org/10.1016/j.jwpe.2020.101380

58. Racchi, M. L., & Camussi, A. (2018). The date palms of Al Jufrah – Libya: A survey on genetic diversity of local varieties. *Journal of Agriculture and Environment in International Development, 112*(1), 161–184. https://doi.org/10.12895/jaeid.20181.776

59. Rambabu, K., AlYammahi, J., Bharath, G., Thanigaivelan, A., Sivarajasekar, N., & Banat, F. (2021). Nano-activated carbon derived from date palm coir waste for efficient sequestration of noxious 2,4-dichlorophenoxyacetic acid herbicide. *Chemosphere, 282*, Article 131103. https://doi.org/10.1016/j.chemosphere.2021.131103

60. Ramesha, G. K., Kumara, A. V., Muralidhara, H. B., & Sampath, S. (2011). Graphene and graphene oxide as effective adsorbents toward anionic and cationic dyes. *Journal of Colloid and Interface Science, 361*(1), 270–277. https://doi.org/10.1016/j.jcis.2011.05.050

61. Rashid, R., Shafiq, I., Akhter, P., Iqbal, M. J., & Hussain, M. (2021). A state-of-the-art review on wastewater treatment techniques: The effectiveness of adsorption method. *Environmental Science and Pollution Research, 28*(8), 9050–9066. https://doi.org/10.1007/s11356-021-12395-x

62. Sanou, I., Bamogo, H., Sanou, A., Ouedraogo, M., Saadi, L., Waqif, M., & Millogo, Y. (2024). Adsorption of methylene blue in aqueous medium by activated carbon from peanut shells. *Chemistry Africa, 7*(6), 2777–2794. https://doi.org/10.1007/s42250-024-00927-0

63. Sghiouri Idrissi, A., Nour Eddine, S., Tayoury, M., Khouya, E. H., El Kacemi, K., & Mouni, L. (2024). Investigation of the regeneration of spent activated carbon from water treatment plants. *International Journal Environmental Science and Technology, 21*(9), 8995–9006. https://doi.org/10.1007/s13762-024-05510-1

64. Si, J., Cui, B. K., Yuan, Y., & Dai, Y. C. (2015). Biosorption performances of raw and chemically modified biomasses from Perenniporia subacida for heterocycle dye Neutral Red. *Desalination and Water Treatment, 57*(18), 8454–8469. https://doi.org/10.1080/19443994.2015.1025439

65. Tenev, M. D., Torre, C., Fontana, G., Gauto, V., Cleva, M. S., Caracciolo, N., & Boeykens, S. (2023). Studies of adsorption–desorption of methylene blue in a fixed-bed reactor filled with cotton and tannin industry waste. In *Proceedings of the 21st LACCEI International Multi-Conference for Engineering, Education, and Technology*. https://dx.doi.org/10.18687/LACCEI2023.1.1.1594

66. Wang, J., Zhang, G., Qiao, S., & Zhou, J. (2021). Magnetic Fe0/iron oxide-coated diatomite as a highly efficient adsorbent for recovering phosphorus from water. *Chemical Engineering Journal, 412*, Article 128696. https://doi.org/10.1016/j.cej.2021.128696

67. Xu, J., Plaxco, K. W., & Allen, S. J. (2006). Probing the collective vibrational dynamics of a protein in liquid water by terahertz absorption spectroscopy. *Protein Science, 15*(5), 1175–1181. https://doi.org/10.1110/ps.062073506

68. Zhou, Q., Wang, X., Tan, X., Zhao, Y., Li, S., & Jin, F. (2024). Selective photocatalytic oxidation of methane to C1 oxygenates by regulating sizes and facets over Au/ZnO. *Nano Research, 17*(5), 3810–3818. https://doi.org/10.1007/s12274-023-6323-5

Information about the authors:

Ashraf El-Hashani – Professor, Dr., Department of Chemistry, Faculty of Science, University of Benghazi (Benghazi, Libya, e-mail: aiiya600@yahoo.co.uk).

Khaled Muftah Elsherif – Associate Prof., PhD, Department of Medical Laboratory Science, Faculty of Health Science, Misurata University (Misurata, Libya, e-mail: elsherif27@yahoo.com).

Ghada F. Musbah – Researcher, University of Benghazi (Benghazi, Libya, email: ghadaghada19943@gmail.com)

Abdelgader Imragaa – Dr., Department of Chemistry, Faculty of Science, University of Benghazi (Benghazi, Libya, e-mail: a.imragaa@uob.edu.ly)

Hanan F. Emrayed – Professor, Chemistry Department, Faculty of Science, Omar Al-Mukhtar University (Al-Bayda, Libya, e-mail: hanan.emrayed@omu.edu.ly)

Received 14 December 2025;
received in revised form 28 December 2025;
accepted 9 June 2026